OUKA
The University of Osaka
Institutional Knowledge Archive

Title	FEM Simulation of Welding Residual Stress in Multi-pass Butt-welded Modified 9Cr-1Mo Steel Pipe Considering Phase Transformation Effects(Mechanics, Strength & Structure Design)
Author(s)	Deng, Dean; Murakawa, Hidekazu; Horii, Yukihiko
Citation	Transactions of JWRI. 2004, 33(2), p. 167-176
Version Type	VoR
URL	https://doi.org/10.18910/4863
rights	
Note	

The University of Osaka Institutional Knowledge Archive : OUKA

https://ir.library.osaka-u.ac.jp/

The University of Osaka

FEM Simulation of Welding Residual Stress in Multi-pass Butt-welded Modified 9Cr-1Mo Steel Pipe Considering Phase Transformation Effects †

DENG Dean*, MURAKAWA Hidekazu **, and HORII Yukihiko***

Abstract

The objective of this paper is to investigate the influence of solid-state phase transformation on the evolution of residual stress distributions in butt-welded modified 9Cr-1Mo steel pipes. A thermal elastic plastic finite element model taking into account the metallurgical phase transformation was developed. Effects on welding residual stress of the volumetric change and the yield strength change due to austenite-martensite transformation were investigated by means of numerical analysis. The results show that the volumetric change and the yield strength change due to martensite transformation have large influences on the welding residual stress. In the case of considering phase transformations, the simulated results are in good agreement with the experimental measurements.

KEY WORDS: (Finite element) (Numerical analysis) (Welding residual stress) (Phase transformation) (Multi-pass welding)

1. Introduction

Welding of the Cr-Mo steels plays a very crucial role in the power and petroleum industries. Hence, welding and post welding heat treatment (PWHT) of the Cr-Mo steels have been extensively studied in recent years [1-6]. Manufacturing processes, such as welding, frequently introduce unwanted residual stress in structures, leading to brittle fracture, hydrogen embrittlement (HE), and a deterioration of fatigue life. Generally, in order to improve the toughness and to remove welding residual stress after welding, the Cr-Mo steel weldment should be subjected to post weld heat treatment. The modified 9Cr-1Mo-alloy steel is a relatively new structural material that was originally developed for steam generators in the advanced nuclear and power generation industry. Because the modified 9Cr-Mo steel has high creep strength, even at high temperature, it needs a relatively high temperature to remove the welding residual stress by PWHT [6]. Thus, to clarify the criteria for suitable PWHT conditions, it is necessary to accurately predict the welding residual stress.

In the context of steels, it has been recognized that phase transformation can significantly affect the development of residual stresses [7, 8]. In order to accurately predict the welding residual stress, metallurgical factor should therefore be taken into account. In this study, our purpose was focused on predicting welding residual stresses in butt-welds for modified 9Cr-1Mo steel pipe considering solid-state phase transformation effects. A thermal elastic plastic finite element model taking into account metallurgical phase transformations was developed. The effects of volumetric change and yield strength change due to austenite-martensite transformation on welding residual stress were investigated by means of numerical analysis. Experiments were also carried out to verify the effectiveness of the proposed numerical model.

2. Experimental Procedure

The material used in this study was modified 9Cr-1Mo steel pipes with outer diameter of 318.5mm, thickness of 21.4mm, and length of 1900mm. Chemical compositions of the base metal and the weld metal, and heat treatment condition of the base metal are shown in **Table 1**. The modified 9Cr-1Mo steel pipe was normalized at 1040°C and tempered at a temperature not lower than 730°C. The pipe was welded by a multi-pass welding method. The sequence of welding pass and the dimensional details of the groove are given in **Figure 1**. The first two passes were performed by gas tungsten arc welding (GTAW) using TGS-9Cb wire as a filler metal. The shielding gas was argon gas. The remaining weld passes were welded by using gas metal arc welding (GMAW) and MGS-9Cb wire as a filler metal. The shielding gas was Ar-5%CO_2. The welding conditions for each pass are shown in **Table 2**.

† Received on December 1, 2004

*Foreign Research Fellow (Chongqing University, China)
**Professor
***JAPEIC

Transactions of JWRI is published by Joining and Welding Research Institute of Osaka University, Ibaraki, Osaka 567-0047, Japan

Table 1 Chemical composition (wt. %) of the base metal and the weld metal and heat treatment condition of the base metal.

Element	C	Si	Mn	P	S	Cr	Mo	V	Nb	N	Al	Ni
Base metal	0.08	0.27	1.29	0.007	0.006	8.86	0.98	0.19	0.03	0.06	0.04	0.38
Weld metal (TIG)	0.07	0.26	0.99	0.008	0.006	8.97	0.90	0.18	0.04	0.022	--	0.68
Weld metal (MIG)	0.07	0.16	0.99	0.007	0.006	8.97	0.90	0.18	0.04	0.022	--	0.68
Normalizing	1040°C/ Furnace cooling											
Tempering	730°C/Air cooling											

Table 2 Welding conditions.

Pass Number	Welding method	Welding current (A)	Arc voltage (V)	Welding speed (cm/min)	Heat input (kJ/mm)	Preheating temperature Inter-pass temperature (°C)
1	GTAW	120	11	5.2	1.52	300
2	GTAW	170	11	6.5	1.73	200-250
3	GMAW	250	30	25.6	1.76	200-250
4	GMAW	250	30	34.0	1.32	200-250
5	GMAW	250	30	33.8	1.33	200-250
6	GMAW	250	30	37.9	1.19	200-250
7	GMAW	250	30	38.9	1.16	200-250
8	GMAW	250	30	34.4	1.31	200-250
9	GMAW	250	30	35.0	1.29	200-250
10	GMAW	250	30	35.3	1.27	200-250
11	GMAW	250	30	40.2	1.12	200-250

After completion of welding, strain gauges with 1mm length were used to measure the welding residual stress on the inside and the outside surfaces where the circumferential angle was 180 degree. **Figure 2** shows the locations of the stress measurement on the inner and the outer surfaces of the welded pipe.

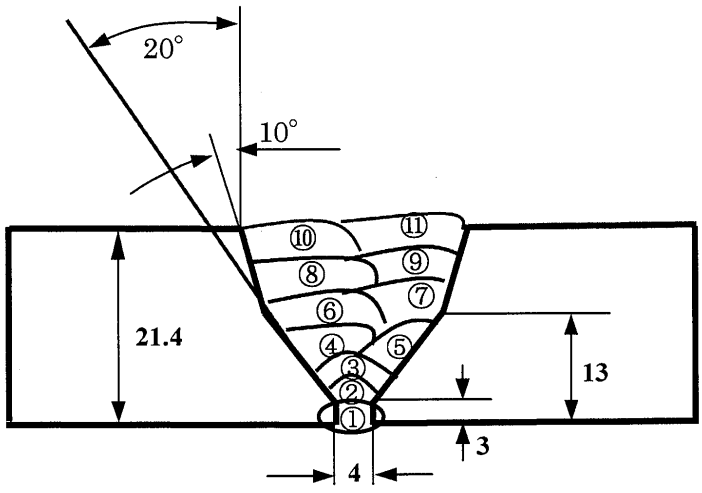

Fig. 1 Dimensional details of the groove and locations of the weld pass.

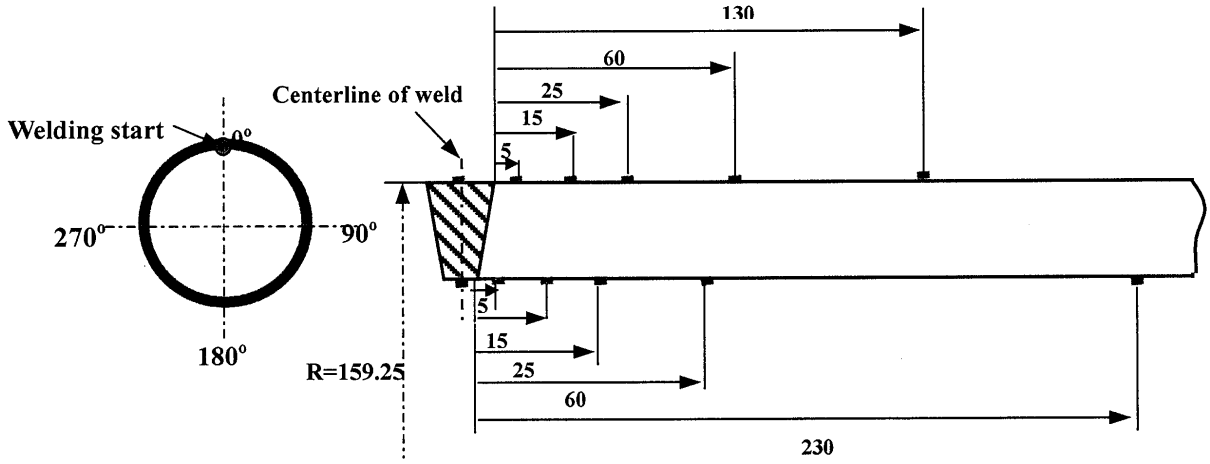

Fig. 2 Measurement locations of the strain gauges along the axial direction.

3. Finite Element Modeling

Fusion welding is a very complicated phenomenon, which includes heat transfer, mass transfer, metallurgical reaction, element diffusion, microstructure change, evolution of mechanical properties and so on. Complex numerical approaches are required to accurately model the welding process. However, to capture all of the aspects will result in a model that cannot always be realistically solved. Some of these factors may not significantly affect the residual stress calculations, and they make the simulation considerably complicated. Therefore, simplifying assumptions should be used to establish a reasonably effective and accurate finite element model.

In this study, the residual stress distribution was simulated by an uncoupled thermo-mechanical finite element formulation using the ABAQUS code [9]. In thermal analysis and mechanical analysis, the computations used temperature dependent thermo-physical and mechanical properties of the base metal and the filler metal. The temperature dependent thermo-physical properties and temperature dependent mechanical properties of the modified 9Cr-1Mo-alloy steel are shown in **Figure 3** and **Figure 4**, respectively. The thermal

analysis was based on the heat conduction formulation with a combined heat source composed of a surface flux and a volumetric flux.

A 3-D finite element analysis is the optimum method of ascertaining the thermal cycle of welding process, but it requires a very long calculation time. Because the heat transfer problem of pipe welding can be simplified to a 2-D axisymmetric analysis by assuming that the welding speed is sufficiently fast relative to the heat conduction rate of the welded metal, an axisymmetric finite element model was developed using linear four-node finite elements.

The main effort was in the development of user subroutines for the ABAQUS code, which were used to simulate the heat input for multi-pass welding in thermal analysis and to incorporate the solid-state phase transformation effects in the mechanical analysis. In the present study, the thermal analysis and the mechanical analysis were uncoupled and conducted in sequence. As a first step, the thermal analysis was carried out computing the transient temperature fields during welding. As a second step, the mechanical analysis was conducted based on the thermal analysis results. In this step, the volume fraction of martensite was also traced using the Koistinen-Marburger relationship. The finite element model employed for the mechanical analysis is similar to the thermal model except for the type of finite element and the boundary conditions.

3.1 Thermal Analysis

The welding model is shown is **Figure 5(a)**, and the sequence of the weld passes is shown in **Figure 5(b)**. The bead size of each weld pass was determined mainly according to the heat input. In the present study, the bead shape was not accurately modeled. The heat input to the work-piece can be divided into two portions, one is the heat of the welding arc, and the other is the heat of the molten metal. In this study, the heat of the welding arc was modeled by a surface heat source with a Gaussian distribution, and that of the molten metal droplets was modeled by a volumetric heat source. The heat of the welding arc was assumed to be 40% of the total heat input, and the heat of the molten metal droplets 60% of the total heat input [10]. In multi-pass welding, new elements were added to the mesh periodically after one weld pass was completed. Meanwhile, the heat transfer boundary conditions were also modified after the new elements were added. To account for heat transfer effects due to fluid flow in the weld pool, an artificial increase in thermal conductivity above the melting temperature was assumed. The thermal effects caused by solidification of the weld pool were modeled by considering the latent heat of fusion. To account for heat losses, both the radiative and convective heat transfers at the work-piece surface were modeled.

The overall heat flux was calculated as:

$$Q=\eta UI \quad (1)$$

Where, η represents the efficiency factor, U is arc voltage, and I is welding current. The efficiency factor is assumed as 0.6 for the GTA welding process, and 0.75 for the GMA welding process. The net heat input of each pass can be calculated according to Table 2.

In the thermal analysis, both preheating temperature and inter-pass temperature were considered. The preheating temperature was assumed to be 300°C, which is the same as in the experiments, and the inter-pass temperature was assumed to be 200±10°C.

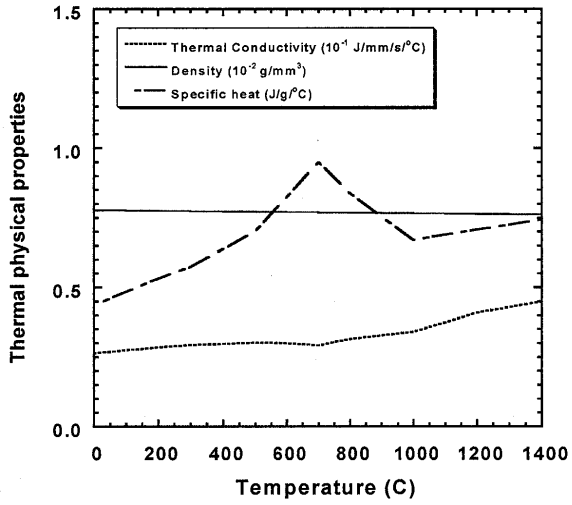

Fig. 3 Temperature dependent thermal physical properties.

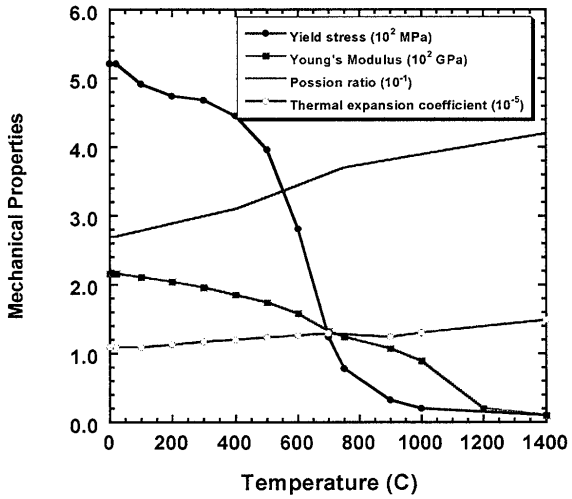

Fig. 4 Temperature dependent thermal mechanical properties.

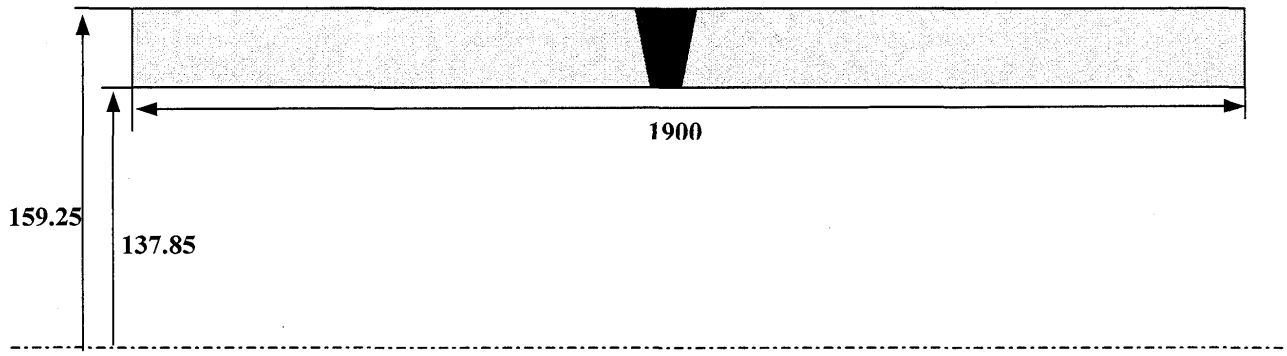

(a) Simulation model

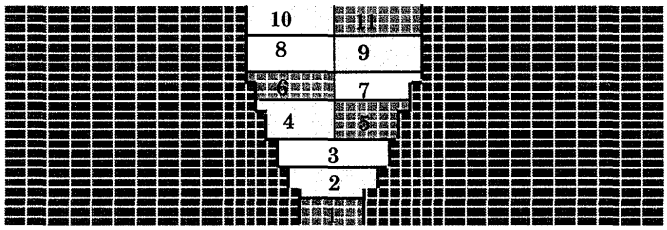

(b) Finite element meshes and sequence of the weld passes

Fig. 5 Simulation model, finite element meshes near the weld zone and sequence of the weld passes.

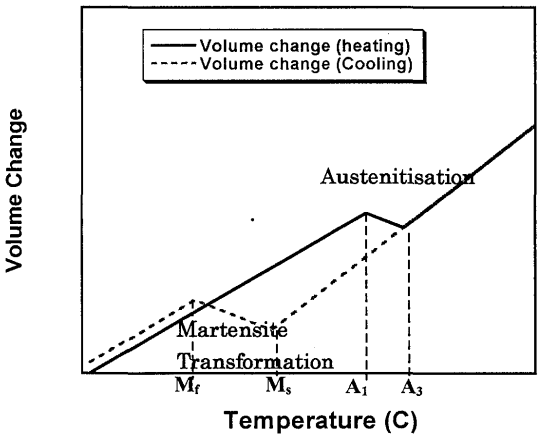

Fig. 6 Schematic diagram of volume change due to phase transformation.

When steel is heated above the A_1 temperature, its body centered cubic (bcc) structure starts to transform to a face centered cubic (fcc) structure, and the volume decreases. During rapid cooling, the austenite with fcc structure changes to martensite with a body centered tetragonal (bct) structure, and the volume increases. The volume change due to phase transformation in the course of heating and cooling is schematically shown in **Figure 6**.

For 9Cr-Mo steel, temperature measurements and calculations show that in spite of the preheating temperature of 300°C and correspondingly large heat input, the metal austenitized during welding cools to 500°C within 100-150 seconds. This cooling time is much smaller than the critical cooling time [11]. This suggests that after weldment cooling to room temperature, the microstructure of the weld metal and the HAZ is full martensite.

The quantity of martensite transformed from austenite depends on the temperature under-cooling below the Ms. This transformation is almost independent of the chemical composition, and takes place in all steel grades.

In this study, depending on the peak temperature that an integration point of an element reached during

heating process and the cooling process from A_3 to 500°C, a decision was made whether the point underwent the austenite to martensite transformation or not. In fact, because the cooling time from A_3 to 500°C is much less than the critical cooling time for the 9Cr-1Mo steel, all points whose peak temperature is higher than A_3 undergo the martensite transformation when cooling to Ms. It was assumed that when cooling to M_f, the austenite completely transforms into martensite.

In the calculations, the M_s temperature was assumed to be 375°C, M_f temperature 200°C, A_1 820°C and A_3 920°C, respectively.

In this study, the Koistien-Marburger relationship [12] expressed by Eq. 2 was used to describe the martensite transformation.

$$f_m = 1 - \exp(-0.011(M_S - T)) \qquad (T \le M_S) \qquad (2)$$

Where, f_m is the fraction of martensite at current temperature; T is the current temperature during cooling.

In order to trace the formation of martensite during cooling, the differential equation based on Eq. 2 was used in the finite element model. Written in the form of increments, the differential equation can be expressed as follows:

$$\Delta f_m = \{-0.011 \exp[0.011(T - M_s)]\} \bullet \Delta T \qquad (3)$$

Where, ΔT is the temperature increment during cooling.

3.3 Mechanical Analysis

In the mechanical analysis, the effects on the residual stress of volume change and the yield stress change due to martensite transformation were taken into account.

In the course of a welding process, an additional strain is induced by the microstructure evolution during solid-state phase transformation along with the thermal strain. Accompanying microstructure change, transformation induced plasticity is also generated. Therefore, the total strain rate ($\dot{\varepsilon}$) can be written as the sum of the individual components of the strain rate as:

$$\dot{\varepsilon} = \dot{\varepsilon}^E + \dot{\varepsilon}^P + \dot{\varepsilon}^T + \dot{\varepsilon}^{\Delta V} + \dot{\varepsilon}^{Trp} \qquad (4)$$

The components in this equation represent strain rate due to elastic, plastic and thermal loading, volumetric change and transformation plasticity, respectively.

In this study, transformation induced plasticity was not taken into account. Ignoring this component, the strain increment can be expressed by the following equation:

$$\Delta\varepsilon = \Delta\varepsilon^E + \Delta\varepsilon^P + \Delta\varepsilon^T + \Delta\varepsilon^{\Delta V} \qquad (5)$$

The volumetric change of the modified 9Cr-1Mo-alloy steel during martensite transformation was measured by experiment [13]. **Figure 7** shows the relationship between the strain due to volumetric change and temperature for the base metal and the weld metal. From this figure, we can see that the Ms temperature of the base metal is 400°C or so, and that of the weld metal is 350°C or so. The broken line shows the average value for the base metal and the weld metal. In this study, the average value was adopted. From Fig. 7, it can also be seen that the strain due to volume change associated with full martensite transformation assigned to the modified 9Cr-1Mo-steel is approximately 7.5×10^{-3}.

Using the Koistinen-Marburger relationship, the strain increment due to volume change in the course of martensite transformation can be calculated using the following equation:

$$\Delta\varepsilon^{\Delta V} = \Delta f_m \bullet \Delta\varepsilon^{\Delta V*} \qquad (6)$$

Where, $\Delta\varepsilon^{\Delta V*} = 7.5\times10^{-3}$.

On heating, the volume change strain due to austenite transformation was also considered using a linear mode [14].

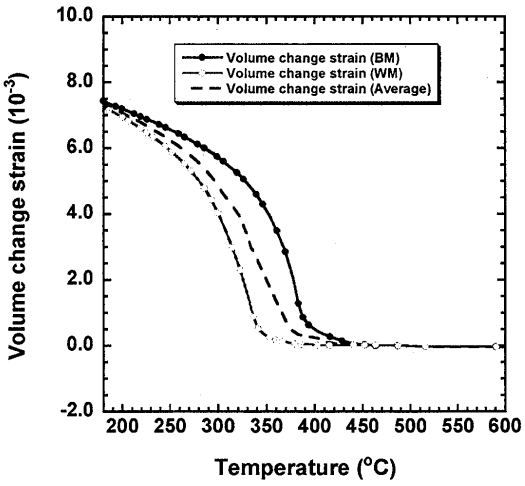

Fig. 7 Volumetric change of modified 9Cr-1Mo steel.

A subroutine to the ABAQUS code was developed to compute the fraction of martensite and volume change during heating and cooling.

Generally, when the microstructure of a material changes during welding process, the mechanical properties such as yield stress and hardness also change. When austenite transforms into martensite in the weld metal and the HAZ, the yield strength in those zones will drastically change. In this study, the yield strength change due to martensite transformation was taken into account. The yield strength of the base metal was employed for the entire model during the first welding (heating). The peak temperature of each integration point in the model was recorded during welding. Depending on the peak temperature that a particular point reached during heating process, the decision was made whether the point underwent the austenite-martensite transformation or not. For each point that underwent the phase transformation the yield strength of the weld metal was applied. For the current weld bead metal, the yield strength of the base metal was used during heating, and when the temperature cooled to the Ms temperature, the yield strength of the weld metal was employed, instead.

Figure 8 shows the temperature dependent yield strength of the base metal and that of the weld metal [13]. The microstructure of the base metal is tempered martensite, and the microstructure of the weld metal untempered martensite. Because of the different microstructures, the yield strength of the base metal is much different from that of the weld metal.

4. Simulated Cases

To clarify the influences on welding residual stress of volumetric change and yield strength change due to martensite transformation, four different cases were studied. In case A, phase transformation was not considered. This means that neither volumetric change nor yield strength change was taken into account. In case B, only the volumetric change due to phase transformation was taken into account, but the yield strength change was neglected. By contrast, in case C, only the yield strength change was involved, but the volumetric change was excluded. In case D, both the volumetric change and the yield strength change were considered. These four simulated cases are shown in **Table 3**.

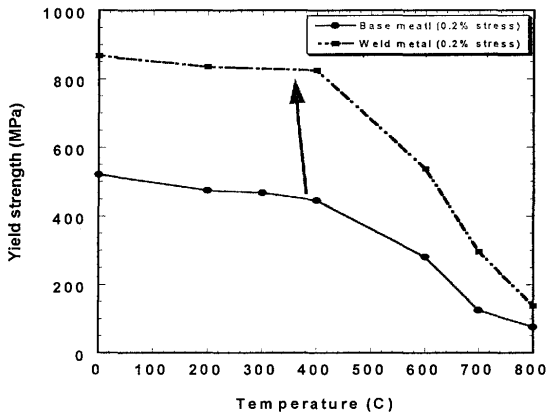

Fig. 8 Yield strengths of the base metal and the weld metal.

5. Results and Discussion

5.1 Influence of Volumetric Change

If case A is assumed as the standard case, by comparing case B and case A, the influence of volumetric change due to martensite transformation can be clarified. **Figure 9** shows the hoop stress in case A and case B on the outer surface. In case A, there is a tensile hoop stress in the fusion zone and the HAZ, and the maximum stress is 520MPa, which is close to the yield strength at room temperature. In case B, it is clear that compressive hoop stress was produced in the fusion zone and the HAZ. The compressive stresses were produced by the volume change due to a relatively low temperature martensite transformation. **Figure 10** shows the axial stress distributions on the outer surface in case A and case B. It can be observed that there is a big difference between the two cases near the weld zone. In case A, compressive stress was generated at the left side of the weld zone, and relatively large tensile stresses were generated at the both sides near the weld zone. In contrast, relatively large compressive stresses were produced at and near the weld zone in case B.

From the simulation results, it can be concluded that the volume change due to martensite transformation has a significant effect on the welding residual stress in the modified 9Cr-Mo steel pipe.

Table 3 Simulated cases.

Case	Volumetric change	Yield strength change
Case A	No	No
Case B	Yes	No
Case C	No	Yes
Case D	Yes	Yes

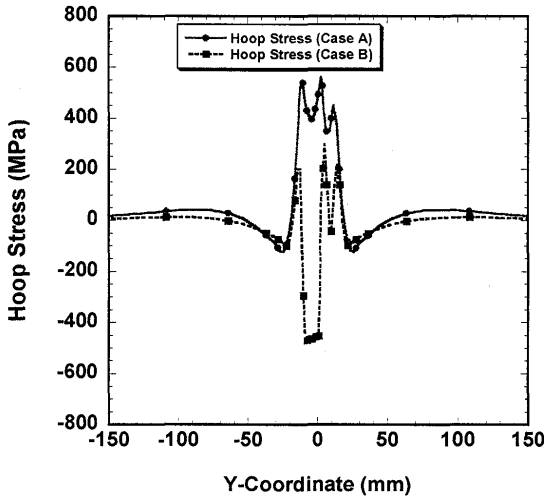

Fig. 9 Hoop stress distributions of case A and case B on the outer surface.

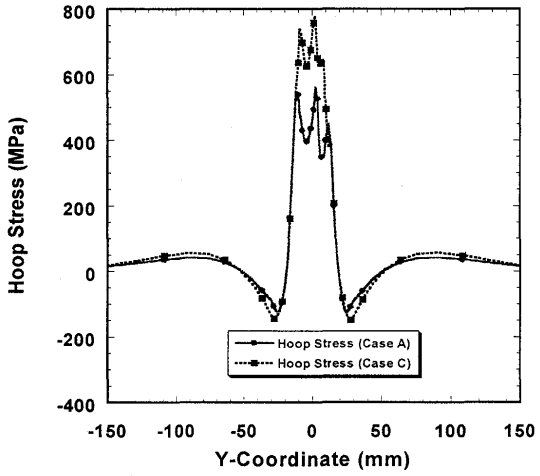

Fig. 11 Hoop stress distributions of case A and case C on the outer surface.

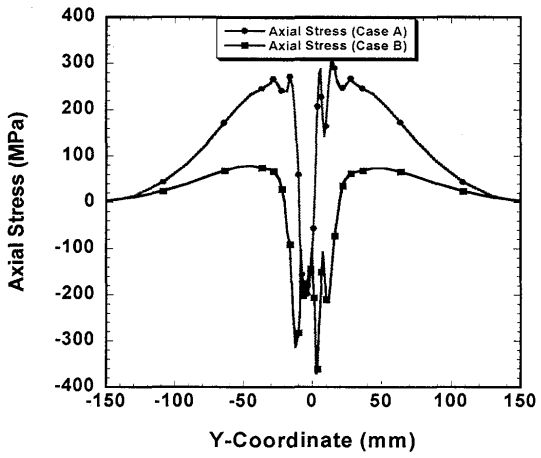

Fig. 10 Axial stress distributions of case A and case B on the outer surface.

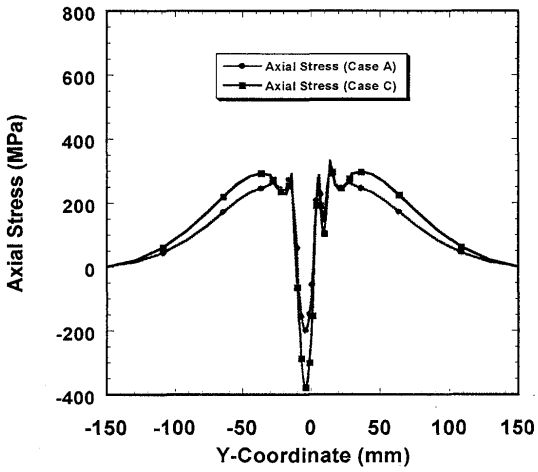

Fig. 12 Axial stress distributions of case A and case C on the outer surface.

5.2 Influence of Yield Strength Change

Figure 11 shows the hoop stresses in case A and case C on outer surface of the pipe. From this figures, one can observe that a higher tensile hoop stress was produced in the weld zone in case C. **Figure 12** shows the axial stress distributions along the axial direction on outer surface in cases A and case C. It can be clearly seen that a higher compressive axial stress is generated at the fusion zone and the HAZ in case C. Because of high yield strengths due to martensite transformation in case C, correspondingly, larger residual stresses were produced after welding. According to simulation results, it is very clear that the yield strength has a marked effect on the welding residual stress.

5.3 Comparison between Simulated Results and Experiment

Figures 13 (a) and **(b)** show the hoop stress distribution of the cases A, B, C and D and the experimental results on the outer and the inner surfaces, respectively. In Fig. 13(a), the stress distributions of case A and case C are very different from those of case B and case D. Compressive stresses were produced in case B and case D due to the volume change induced by martensite transformation. The stresses measured by strain gauge method are in a good agreement with those of case B and case D. The results predicted in case A and case C are much different from the experimental results. From Fig.13 (b), one can observe that expect for a relatively large tensile hoop stress

predicted by case B and case D in the weld zone, the stresses in other locations are in a good agree with those of experiment. Similar to the stress distributions on the outer surface, there are large differences between the cases A, C and the experiment in the inner surface.

Figures 14(a) and **(b)** show the axial stress distribution of the cases A, B, C and D and the experimental results on the outer and the inner surfaces, respectively. In Figs. 14 (a) and (b), it can be observed that the axial stress distributions of the cases A and C are much different from those of the cases B and D. This figure also shows that the stresses predicted in the cases B and D are in a good agreement with the experimental results.

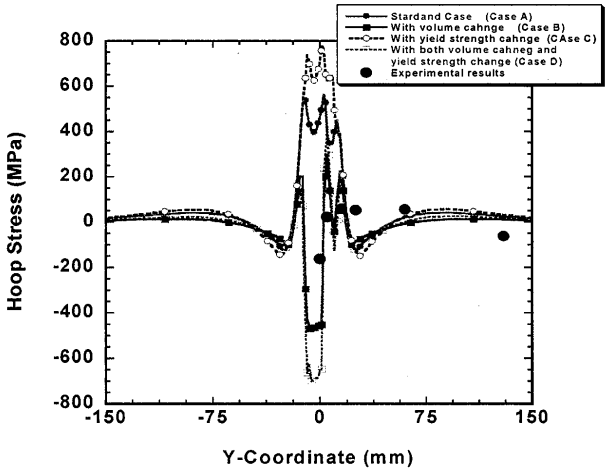

(a) Outer surface

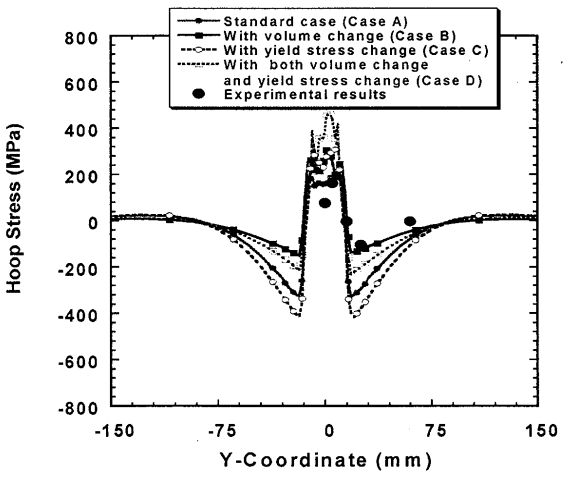

(b) Inner surface

Fig. 13 Hoop stress distributions in the axial direction.

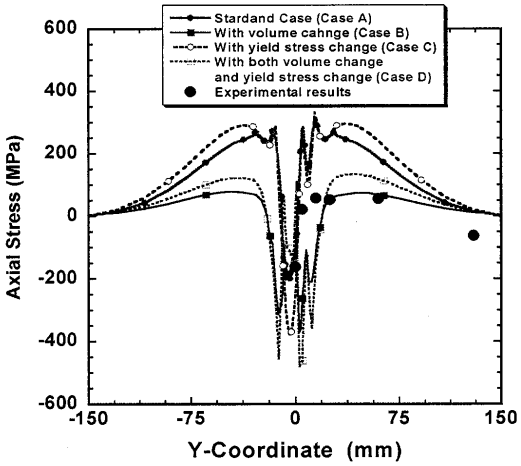

(a) Outer surface

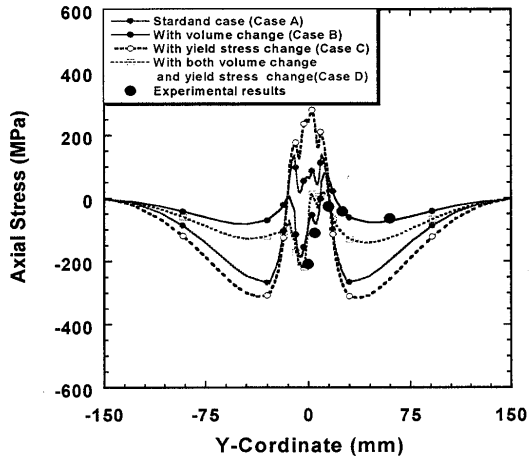

(b) Inner surface

Fig. 14 Axial stress distributions in the axial direction.

Comparing the simulation results and the experimental results, one can conclude that in such analyses even through the yield strength has some effect on welding residual stress, it is not so important to account for the yield strength due to martensite transformation, as it is to consider the volumetric change in the weld zone caused by austenite to martensite transformation. This means the influence induced by volume change is more significant than that due to yield strength change. The former make both the sign and the magnitude of the residual stress change, and the latter only produce the change of stress in magnitude.

Through carefully comparing the experimental

results and the simulated results of case B and case D, one can find that the simulated results of case B are closer to the experimental results. The reason can be that an overestimated yield stress was used in case D. In case D, at those locations, whose peak temperature was higher than the A_3 temperature and cooled down to the **Ms** temperature, high yield strength was employed in the simulation. In fact, in the course of solid-state phase transformation, the microstructure was a mixture composed of austenite and martensite. With the temperature decreasing, the fraction of each phase changes and hence the yield strength also changes. In case D, when the temperature cooled to Ms, the yield stress of the untempered martensite was applied instead of the yield strength of the base metal. Moreover, in multi-pass welding, the original weld pass is tempered by the successive weld passes. After tempering, the yield strength of material will decrease. Therefore, it caused a problem that the yield stress is overestimated in case D.

6. Conclusions

A finite element model for welding residual stress analysis, which takes into account the volumetric change and yield strength change due to martensite transformation, was developed. The proposed method was used to predict the welding residual stress in modified 9Cr-1Mo-alloy steel pipe by multi-pass welding method, and the following conclusions have been drawn.

(1) The proposed numerical model considering marteniste transformation was effectively applied to the analysis of residual stress in multi-pass welding.

(2) According to the simulation results, it is clear that the volume change due to marteniste transformation has a significant influence on welding residual stress. It not only changes the magnitude of the residual stress, but also alters the sign of residual stresses in the weld zone.

(3) The yield strength change induced by solid-sate phase transformation also has a marked effect on the welding residual stress.

(4) When the volume change due to martensite transformation is taken into account, the finite element simulation results are generally in good agreement with the strain gauge experimental results.

(5) Because of a relatively low Ms temperature and relatively large volume dilation in modified 9Cr-1Mo-alloy steel, it is necessary to consider the effects of martensite transformation in the analysis of welding residual stress.

References

1) Grandy D. W, Findlam S.J. and Viswanathan R., J. of Pres. Ves. Tech., Vol.123 (2001), pp.157
2) Viswanathan R.and Gandy D. W., J.of Mat. Eng. And Perf., Vol. 8(5), 1999, pp.579
3) Nonaka I., Ito T., Ohtsuki S. and Takagi Y., Int. J. of Pres. Ves.and Piping, 78(2001), pp.807
4) H.O. Andren, G.. Cai, and L.E. Svensson, Appl. Surf. Sci. 87/88(1995), pp.200
5) K. Laha, K.S. Chandravathi, K.B.S.Rao, et al, Int.J. of Pres. Ves. And Piping, 77(2000), pp.761
6) S. Nishikawa, Y. Horii, H. Murakawa, H. Lu, J. Tanaka, J. weld. Soci. (2002), pp.366
7) B. Taljat, B.Radhakrishnan, T.Zacharia, Mater.Sci. Eng. A246(1998), pp.45
8) H.K.D.H.Bhadeshia, Mater.Sci.Eng. A 378(2004), pp.34
9) Hibbitt, Karlsson, Sorensen, ABAQUS/Standard Useris Manual, Vol.1,2, 3, Version 6.3
10) E.Pardo, D.C. Weckman, Metal. Trans. B Vol.20B (1989), pp.937
11) L.Beres, A.Balogh, W.Irmer, Weld. J, 2001, pp.191s
12) G.Krauss, Principles of Heat Treatment of Steel. Materials Park, Ohio, ASM International.
13) Japan Power Engineering and Inspection Corp. Research Report (2002).
14) Deng Dean, Luo Yu, Serizawa Hisashi, Shibahara Masakazu and Murakawa Hidekazu, Trans. JWRI, Vol.32 (2), 2003, pp.325